Using Series-Series Iwan-Type Models for Understanding Joint Dynamics

D. Dane Quinn
Department of Mechanical Engineering,
The University of Akron,
Akron, OH 44325-3903
e-mail: quinn@uakron.edu

Daniel J. Segalman[1]
Sandia National Laboratories,
P. O. Box 5800, MS 0847,
Albuquerque, NM 87185-0847
e-mail: djsegal@sandia.gov

In mechanical assemblies, the energy loss induced by joints and interfaces can account for a significant portion of the overall structural dissipation. This work considers the dynamical behavior of an elastic rod on a frictional foundation as a model for the dissipation introduced by micro-slip in mechanical joints. In a quasi-static loading limit, the deformation of the rod and hence the frictional dissipation can be solved in closed form. The resulting model is a continuum model of series arrangements of parallel Jenkins elements. For a general class of normal load distributions, the resulting energy loss per forcing cycle follows a power-law and is qualitatively similar to observed experimental findings. Finally, these results are compared with those obtained from a discrete formulation of the rod including inertial effects. For loading conditions that are consistent with mechanical joints, the numerical results from the discrete model are consistent with the closed form predictions obtained in the quasistatic limit. [DOI: 10.1115/1.1978918]

1 Introduction

In many structures of great engineering importance, such as air frames or jet engines, the primary source of vibration damping is often just the frictional damping of interfaces associated with mechanical joints. This damping is associated with slip in outer regions of the contact patches and is known to be strongly amplitude dependent (and hence nonlinear) [1,2]. These mechanisms have traditionally been accommodated in structural dynamics only indirectly. For instance, one may use a finite element code to deduce modes and frequencies but then wait for data taken from a prototype tested at amplitudes of interest to obtain nominal values for modal damping coefficients.

As the need and expectation of *predictive* structural dynamics simulation grows, the requirement of systematically accounting for the role of joints in the structural response becomes more urgent [3]. Unfortunately, the most direct method of accommodating joint mechanics into finite element analysis—meshing the joint regions finely enough to capture any relevant micromechanics [4,5]—proves to be impractical for large-scale structural systems because of the prohibitively small time steps required and/or matrix ill-conditioning that results from the attempt to resolve the interfaces. A more practical approach is to devise constitutive models for the overall behavior of individual joints and to incorporate that constitutive response locally into the structural model. In the following we discuss a class of models that captures important qualitative properties of mechanical joints in a manner that can be integrated into conventional finite element codes.

The qualitative behavior generally found for joints is illustrated by two types of experiments. The first is a unidirectional lateral pull test. At small loads, the force-displacement curve appears linear, though some amount of micro-slip in the interface does take place. At larger loads, as slip increases, the curve begins to level out and finally, at macro-slip the curve becomes flat. Of course, if there is a bolt at the core of the joint, that bolt will eventually come into shear and a new apparently linear portion of the curve begins.

The second experiment that illustrates the core features of joint response is a lap joint subject to small amplitude lateral oscillatory loads. When energy dissipation per cycle is plotted against the force amplitude on a log-log scale, the result is generally well-approximated by a straight line, whose slope lies between 2.0 and 3.0 [6,7]. (It is interesting to note that Goodman pointed out forty years ago that the Mindlin solution for spheres pressed together and subject to similar *small* oscillatory loads predicts similar power-law dissipation with a slope of 3 [8].) Though the departure of power-law slope of experimental values from the Goodman value of 3.0 has often been ascribed to nonlinear material response [2], recent work [5] indicates that the slope may also depend on geometric nonlinearities reflective of the geometry of the joint.

This paper considers a simplified model for the prediction of energy dissipation in mechanical joints and interfaces. The model represents an elastic rod on a frictional foundation with time-varying shear loads and spatially varying normal pressure. In the quasi-static limit, these continuum equations are solved in closed form to determine the force-displacement relationship and thereby deriving an expression for the energy dissipation per cycle of harmonic forcing. Finally, the continuum model is discretized and the resulting n-dof model is studied for non-zero forcing frequency and as the model order n varies.

Iwan Models. Iwan considered two permutations of a spring and frictional damper—arranged in series and connected in parallel, sometimes referred to as Jenkins elements [9,10] (see Fig. 1). The parallel element allows for changes in force with zero change in displacement while the series element allows for changes in displacement with zero force change. Moreover, researchers including Iwan have considered both series and parallel collections of each of these elements. This gives rise to four combinations: series arrangements of parallel elements (series-parallel), series-series, parallel-parallel, and parallel-series. Of these, the most well-known systems are parallel arrangements of series elements. In this configuration, all spring stiffnesses are set to be identical, the sliders are all connected to ground, and the left node is left

[1]Sandia is a multi-program laboratory operated by Sandia Corporation, a Lockheed Martin Company, for the United States Department of Energy under Contract No. DE-AC04-94AL85000.

Contributed by the Applied Mechanics Division of THE AMERICAN SOCIETY OF MECHANICAL ENGINEERS for publication in the ASME JOURNAL OF APPLIED MECHANICS. Manuscript received by the Applied Mechanics Division, January 3, 2003; final revision, August 10, 2004. Associate Editor: A. A. Ferri. Discussion on the paper should be addressed to the Editor, Prof. Robert M. McMeeking, Journal of Applied Mechanics, Department of Mechanical and Environmental Engineering, University of California - Santa Barbara, Santa Barbara, CA 93106-5070, and will be accepted until four months after final publication in the paper itself in the ASME JOURNAL OF APPLIED MECHANICS.

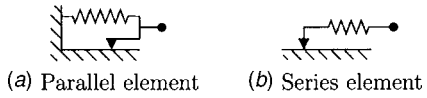

Fig. 1 Iwan elements

free. Iwan's parallel-series network has had some popularity, primarily because of equations that Iwan presented to deduce model parameters in terms of gross force-displacement behavior [11]. A similar analysis has not been available for the series-parallel system, and it has been generally assumed that the parallel-series network is unique in having the useful relationships between model parameters and gross behavior.

Iwan's equations for the deduction of parameters for a parallel network employs the force-displacement curve from monotonic loading for the boundary of the system. We show in the following that similarly useful relations can be obtained for another of the four permutations of Iwan network types: the series-series network. In the following, we do our best to derive equivalent expressions for the above-defined series-series system. In particular, the series-series arrangement provides a straightforward point of departure for considering the dynamical behavior of mechanical joints. In this work we attempt to relate the characteristics of these simplified models to experimentally observed behavior from mechanical lap joints as well as simulations based on a discrete model for a rod on a frictional foundation.

Physical model. The physical model under consideration can be described as a uniform elastic rod of length L held in place by a frictional surface, as illustrated in Fig. 2. The continuum model for this system can be written as

$$\rho\frac{\partial^2\tilde{u}}{\partial\tilde{t}^2}(\tilde{x},\tilde{t}) - EA\frac{\partial^2\tilde{u}}{\partial\tilde{x}^2}(\tilde{x},\tilde{t}) = \tilde{G}(\tilde{x},\tilde{t}), \tag{1}$$

where $\tilde{u}(\tilde{x},\tilde{t})$ is the lateral displacement of the rod at location $\tilde{x}$ and time $\tilde{t}$ while EA is the rod stiffness. The function $\tilde{G}(\tilde{x},\tilde{t})$ describes the force acting on the rod arising from friction. A Coulomb model is used to describe friction and it is assumed that the coefficient of friction does not vary over the interface. Also, no distinction is made between static and kinetic coefficients of friction. More realistic interface models would necessarily consider generalized descriptions of friction such as mesoscopic asperity based models [12,13] and friction laws dependent on interfacial variables, including slip rate [14]. The Amontons law of friction can be uniquely specified in terms of two quantities: $\mu N(\tilde{x})$, the frictional intensity, and $\mathcal{G}^{\mathrm{eq}}(\tilde{x},\tilde{t})$, the value of the friction force that would be required to maintain static equilibrium in a state of sticking. With these, the friction force is described by

$$\tilde{G}(\tilde{x},\tilde{t}) = \begin{cases} -\mu N(\tilde{x})\mathrm{sgn}(\dot{\tilde{u}}(\tilde{x},\tilde{t})), & \dot{\tilde{u}}(\tilde{x},\tilde{t}) \neq 0, \\ -\min\left(|\tilde{\mathcal{G}}^{\mathrm{eq}}(\tilde{x},\tilde{t})|, \mu N(\tilde{x})\right)\cdot \mathrm{sgn}\left(\tilde{\mathcal{G}}^{\mathrm{eq}}(\tilde{x},\tilde{t})\right), & \dot{\tilde{u}}(\tilde{x},\tilde{t}) = 0. \end{cases} \tag{2}$$

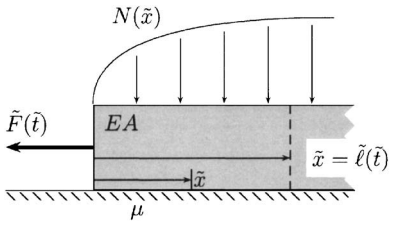

Fig. 2 Physical system. The rod slips over the interval $0 \leq \tilde{x} < \tilde{\ell}(\tilde{t})$.

The frictional intensity $\mu N(\tilde{x})$ is the product of the magnitude of the normal force and the coefficient of friction. Each of these quantities can depend independently on the spatial position along the rod. However, as they appear only in the combination $\mu \cdot N$, we do not differentiate between the $N(\tilde{x})$ and $\mu(\tilde{x})$. The function sgn is the sign of nonzero arguments and zero if its argument is zero. Finally, $\tilde{\mathcal{G}}^{\mathrm{eq}}(\tilde{x},\tilde{t})$, the force required to maintain sticking, is

$$\tilde{\mathcal{G}}^{\mathrm{eq}}(\tilde{x},\tilde{t}) = -EA\frac{\partial^2\tilde{u}}{\partial\tilde{x}^2}(\tilde{x},\tilde{t}) \tag{3}$$

This model is subject to a suitable initial state and a natural boundary condition at $\tilde{x}=0$:

$$\frac{\partial\tilde{u}}{\partial\tilde{x}}(0,t) = \frac{\tilde{F}(\tilde{t})}{EA}, \tag{4}$$

where positive values of $\tilde{F}$ imply the end of the bar is in tension.

We nondimensionalize this model through the transformations:

$$\tilde{x} = L\,x, \quad \tilde{t} = \sqrt{\frac{\rho L^2}{EA}}t, \quad \tilde{u} = \left(\frac{L}{EA}\int_0^L \mu N(\xi)d\xi\right)u,$$

$$\tilde{F} = \left(\int_0^L \mu N(\xi)d\xi\right)F, \tag{5}$$

yielding the following equations:

$$\frac{\partial^2 u}{\partial t^2}(x,t) - \frac{\partial^2 u}{\partial x^2}(x,t) = G(x,t), \quad x \in (0,1) \tag{6}$$

with:

$$G(x,t) = \begin{cases} -\psi(x)\mathrm{sgn}(\dot{u}(x,t)), & \dot{u}(x,t) \neq 0, \\ -\min\left(|\mathcal{G}^{\mathrm{eq}}(x,t)|, \psi(x)\right)\mathrm{sgn}(\mathcal{G}^{\mathrm{eq}}(x,t)), & \dot{u}(x,t) = 0, \end{cases} \tag{7}$$

where $\psi(x)$ represents the frictional intensity and in terms of dimensional quantities:

$$\psi(x) = \frac{\mu N(L\,x)L}{\displaystyle\int_0^L \mu N(\xi)d\xi} \tag{8}$$

Finally, the boundary condition at $x=0$ can be written as

$$\frac{\partial u}{\partial x}(0,t) = F(t) \tag{9}$$

A few words concerning this nondimensionalization are in order. The frictional intensity satisfies the constraint:

$$\int_0^1 \psi(\xi)d\xi = 1, \tag{10}$$

which implies that the interface can support a maximum total (nondimensional) friction force of one. Also, the nondimensional length of the rod is now unity and time has been scaled by the period required for a longitudinal wave to traverse the interface. For typical applications, the joint is expected to extend over a very small interval and therefore the corresponding frequency will be much larger than typical frequencies associated with the forcing $\tilde{F}(\tilde{t})$. In terms of the nondimensional time t, the forcing frequencies are expected to be much less than one. Consequently, in many problems of interest the results do not depend on inertia, but the presence of inertial terms stabilizes the numerical results. Likewise, the dimensional forcing amplitude has been scaled by the force required to induce gross slip in the interface. Realistic amplitudes of the nondimensional forcing F are usually expected to be much less than one for most structural problems.

2 Continuum Results

A closed form solution to the continuum problem is unavailable in terms of elementary functions due to the nonlinear form of the interfacial friction, except for the case $\rho=0$, which we consider in the following. Under nonzero external force with $|F|<1$, there exists an interval $0\leqslant x<\ell(t)$ over which the interface exhibits slip. We further assume that for the non-slip region, that is, $x>\ell(t)$, the displacement profile of the rod is specified. In particular the quantities:

$$u(\ell(t),t), \quad \frac{\partial u}{\partial x}(\ell(t),t) \tag{11}$$

are known. Neglecting the inertial terms in the above-noted differential equation, over the interval of slip the deformation of the rod is described as

$$\frac{\partial^2 u}{\partial x^2}(x,t) = \psi(x)\ \mathrm{sgn}(\dot{u}(x,t)), \tag{12}$$

while the boundary condition at $x=0$ remains unchanged. Finally, because of the quasi-static approximation (and sign conventions) the velocity of slip has sign opposite to the term $\dot{F}$, that is:

$$\mathrm{sgn}\big(\dot{u}(0,t)\big) = \mathrm{sgn}\big(-\dot{F}(t)\big) \equiv \sigma(t) \tag{13}$$

It is worth noting that this model is closely related to the Menq model [15,16], which generalizes the frictional interface considered here to an elastoplastic shear layer at the interface. However, the present model incorporates spatial variations in the frictional intensity, whereas the Menq model considers only uniform pressure.

2.1 General Response. We consider general loading conditions applied at $x=0$. Integration of the governing equation and application of the boundary conditions yields

$$\frac{\partial u}{\partial x}(x,t) = F(t) + \sigma(t)\int_0^x \psi(s)ds, \tag{14a}$$

$$u(x,t) = u(\ell(t),t) - F(t)\big(\ell(t)-x\big) - \sigma(t)\int_x^{\ell(t)}\int_0^s \psi(\xi)d\xi\, ds. \tag{14b}$$

The integral of $\psi(x)$ will appear throughout the following analysis. Therefore to simplify the resulting expressions we identify

$$\int_0^x \psi(\xi)d\xi \equiv \Psi(x), \tag{15}$$

and we note that $\Psi(0)=0$. In addition, because of the nondimensionalization $\Psi(1)=1$ (see Eq. (10)). Physically, $\Psi(x)$ represents the total frictional loading over the interval $[0,x)$, provided the interval is uniformly slipping. Therefore the above-noted solutions are written as

$$\frac{\partial u}{\partial x}(x,t) = F(t) + \sigma(t)\Psi(x), \tag{16a}$$

$$u(x,t) = u(\ell(t),t) - F(t)\big(\ell(t)-x\big) - \sigma(t)\int_x^{\ell(t)}\Psi(s)ds. \tag{16b}$$

Evaluating Eq. (16*a*) at $x=\ell(t)$, we find

$$\frac{\partial u}{\partial x}(\ell(t),t) = F(t) + \sigma(t)\Psi(\ell(t)), \tag{17}$$

and evaluating Eq. (16*b*) at $x=0$, the displacement at the end of the rod is seen to be

$$u(0,t) = u(\ell(t),t) - F(t)\ell(t) - \sigma(t)\int_0^{\ell(t)}\Psi(s)ds \tag{18}$$

Moreover, the gradient of this terminal displacement with respect to the external load is simply:

$$\frac{d}{dF(t)}\big(u(0,t)\big) = -\ell(t) \tag{19}$$

2.2 Unidirectional Loading.

2.2.1 Slip Zone. On unidirectional loading from an initially undeformed state, we anticipate a region of slip of length $\ell_1(t)$, in which the deformation gradient at $x=0$ reflects the external force $F(t)=f_1(t)$. (In the following description the subscript "1" indicates the initial loading into the undeformed material.) At the other end of the slip region, the displacement is zero. Also, because the right-hand side abuts an undeformed domain, the force there must be zero also. Therefore:

$$\frac{\partial u_1}{\partial x}(0,t) = f_1(t), \quad u_1(\ell_1,t) = 0, \quad \frac{\partial u_1}{\partial x}(\ell_1,t) = 0, \tag{20}$$

where $u_1(x,t)$ is the displacement field resulting from the application of $F(t)=f_1(t)$.

Applying these boundary conditions we find

$$f_1(t) = -\sigma_1(t)\Psi(\ell_1(t)), \tag{21}$$

and the displacement at $x=0$ may be reduced to

$$u_1(0,t) = \sigma_1(t)\left[\ell_1(t)\Psi(\ell_1(t)) - \int_0^{\ell_1(t)}\Psi(s)ds\right] \tag{22}$$

with $\sigma_1(t)=\mathrm{sgn}(-\dot{f}_1(t))$.

As in Iwan's original work, we may relate the force-displacement curve to the model parameters, in this case the distribution of the normal force over the interface. Making repeated use of the chain rule for differentiation, we obtain

$$\frac{d}{df_1(t)}\big(u_1(0,t)\big) = -\ell_1(t), \tag{23}$$

as above, and differentiating again, using the definition of $\Psi(x)$:

$$\frac{d^2}{df_1^2}\big(u_1(0,t)\big) = \frac{1}{\psi(\ell_1(t))} \tag{24}$$

Knowledge of the force-displacement curve generated by unidirectional loading into undeformed material can be used to identify the tangential tractions acting at the interface. In practice, Eq. (24) typically yields reliable estimates for ψ only for large arguments since $\partial^2 u_1/\partial f_1^2$ is hard to evaluate meaningfully for small argument.

2.2.2 Power-Law Scalings of Dissipation. Say in the vicinity of $x=0$, the frictional intensity can be described as $\psi(x)=(\alpha+1)x^\alpha$, or equivalently:

$$\Psi(x) = x^\beta, \tag{25}$$

with $\alpha=\beta-1$. The solution to Eq. (16), subject to unidirectional loading is

$$\frac{\partial u_1}{\partial x}(x,t) = f_1(t)\left[1-\left(\frac{x}{\ell_1(t)}\right)^\beta\right], \tag{26a}$$

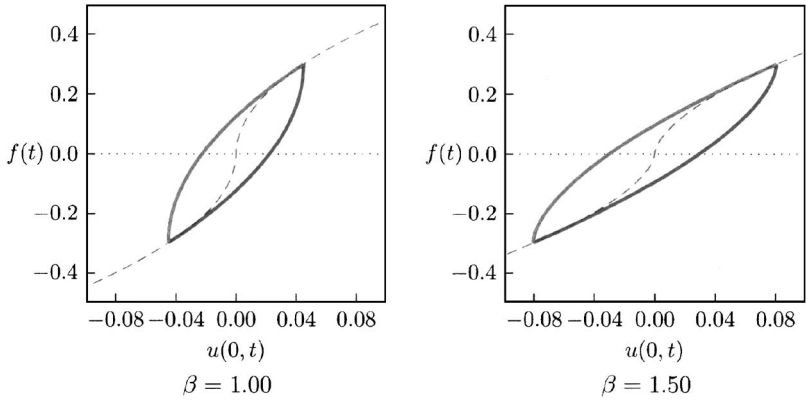

Fig. 3 Force-displacement curve. The dashed curve represents the force-displacement curve generated from loading into undeformed material [Eq. (28)]. In each panel the loading amplitude is 0.30.

$$u_1(x,t) = f_1(t)\ell_1(t)\left[\frac{1}{\beta+1}\left(1-\left(\frac{x}{\ell_1(t)}\right)^{\beta+1}\right)-\left(1-\frac{x}{\ell_1(t)}\right)\right], \tag{26b}$$

with

$$\ell_1(t) = (|f_1(t)|)^{1/\beta} \tag{27}$$

Consequently, the deformation of the rod can be written as

$$u_1(0,t) = \frac{\beta}{\beta+1} f_1(t)|f_1(t)|^{1/\beta} \tag{28}$$

(The above presented equations apply equally for tensile loading on the free surface.)

We now observe that the energy dissipation D due to small oscillatory loads is four times the dissipation due to a single monotonic loading of the same amplitude:

$$D = 4\int_0^{\ell_1(t)} u_1(x,t)\psi(x)dx = \frac{4\beta}{(\beta+1)(2\beta+1)} f_1(t)^{2+1/\beta}. \tag{29}$$

This last result is very interesting. If we associate the frictional intensity $\psi(x)$ with the normal traction in contact and recall that in Hertzian contact the normal traction goes as $\sqrt{x}$, then we set $\beta = 3/2$. In that case, the dissipation goes as $f_1^{8/3}$, which is reasonably close to the experimental values.

2.3 Cyclic Loading. Say that after we have pushed the rod by a force $F(t)=f_1^*$ to obtain slip out to a length ℓ_1^*, we then reduce the applied load, indicated as $F(t)=f_2(t)$. Reduction of the loading induces a new slip zone initiating at the free end of the rod. Notice that from Eq. (19), at the instant of this reversal the stiffness of the rod is infinite. Labeling the length of that new slip zone as $\ell_2(t)$, within that slip zone, the governing equation remains unchanged. However, $\sigma_2=-\sigma_1^*$ and the relevant boundary conditions for the deformation gradients become

$$\frac{\partial u_2}{\partial x}(0,t) = f_2, \tag{30a}$$

$$\frac{\partial u_2}{\partial x}(\ell_2(t),t) = \frac{\partial u_1^*}{\partial x}(\ell_2(t)) = f_1^* + \sigma_1^*\Psi(\ell_2(t)), \tag{30b}$$

where $u_1^*(x)$ represents the deformation profile of the rod at the point of reversal. The length $\ell_2(t)$ of the new slip zone can be found from Eq. (16a) subject to the above-noted boundary conditions, from which one finds

$$f_2(t) + \sigma_2\Psi(\ell_2(t)) = f_1^* + \sigma_1^*\Psi(\ell_2(t)) \tag{31}$$

Therefore, solving for the length of the new slip zone:

$$\ell_2(t) = \Psi^{-1}\left(\frac{f_1^* - f_2(t)}{2\sigma_2}\right), \tag{32}$$

provided of course that $\ell_2(t) < \ell_1^*$. Recalling Eq. (19), the force-displacement curve can be determined to be

$$\int_{f_1^*}^{f_2(t)} \left\{\frac{du(0,t)}{df(t)} = -\Psi^{-1}\left(\frac{f_1^* - f_2(t)}{2\sigma_2}\right)\right\} df_2(t), \tag{33}$$

$$u(0,t)\big|_{f_2(t)} = u(0,t)\big|_{f_1^*} - \int_{f_1^*}^{f_2(t)} \Psi^{-1}\left(\frac{f_1^* - f_2(t)}{2\sigma_2}\right) df_2(t). \tag{34}$$

For our power-law representation of the frictional intensity, we find

$$\ell_2(t) = \left(\frac{f_1^* - f_2(t)}{2\sigma_2}\right)^{1/\beta}, \tag{35}$$

and therefore the force-displacement curve takes the form

$$u(0,t)\big|_{f_2(t)} = u(0,t)\big|_{f_1^*} - \frac{2\beta}{\beta+1}\sigma_1^*\left(\frac{f_1^* - f_2(t)}{2\sigma_2}\right)^{1+1/\beta}. \tag{36}$$

Over a harmonic cycle of loading, we obtain hysteresis curves as illustrated in Fig. 3 for $\beta=1.00$ and $\beta=1.50$. In addition, the above-presented description of the force-displacement curve can be applied to more general loading conditions.

2.4 Relationship With Parallel-Series Models. We briefly review the force-displacement response of parallel-series system. Iwan showed ([10,11]) that for a parallel-series system (continuum of series elements in parallel) all having the same spring stiffness k, but a distribution $\tilde{\rho}(\tilde{\phi})$ of sliders of strength $\tilde{\phi}$, the instantaneous force-displacement relationship is

$$\tilde{F}(\tilde{u}(t)) = k\int_0^\infty \tilde{\rho}(\tilde{\phi})\left[\tilde{u}(t) - \tilde{x}_{\tilde{\phi}}(t)\right]d\tilde{\phi}, \tag{37}$$

where $\tilde{u}(t)$ is the imposed extension and $\tilde{x}_{\tilde{\phi}}(t)$ is the displacement of sliders of strength $\tilde{\phi}$ at time t.

The break-free force of the system is that which can cause gross slip to occur:

$$\bar{\phi} = \int_0^\infty \tilde{\phi}\tilde{\rho}(\tilde{\phi})d\tilde{\phi} \tag{38}$$

Equation (37) is nondimensionalized by dividing both sides by break-free force $\bar{\phi}$ and scaling the displacements by $\bar{\phi}/k$:

$$F(u(t)) = \int_0^\infty \rho(\phi)\left[u(t) - x_\phi(t)\right]d\phi, \tag{39}$$

where $\phi = \tilde{\phi}/\bar{\phi}$ and $\rho(\phi) = \bar{\phi}\tilde{\rho}(\bar{\phi}\phi)$. Note that the above also normalized ρ:

$$\int_0^\infty \phi\ \rho(\phi)d\phi = 1, \tag{40}$$

implying that gross slip occurs at an applied load of $F=1$.

As in the previous analysis, as this Iwan system is loaded from the underformed state, the slider displacements can be deduced to be as follows:

$$x_\phi(t) = u(t) - \phi \text{ for all } \phi < |u(t)|, \tag{41}$$

and

$$x_\phi(t) = 0 \text{ for all } \phi \geqslant |u(t)| \tag{42}$$

At this initial state we now break the above-presented force integral into two parts:

$$F(t) = \int_0^{u(t)} \phi\ \rho(\phi)d\phi + K_u u(t), \tag{43}$$

where

$$K_u = \int_{u(t)}^\infty \rho(\phi)d\phi \tag{44}$$

The quantity K_u represents the elastic stiffness arising from those elements which do not undergo slip during this loading.

Having achieved a displacement u^* with a force F^*, we now consider the force response as the system is reversed. For each spring-slider unit, characterized by the value of ϕ, the response is initially elastic as $u(t)$ withdraws from $u^*$to $u^* - 2\phi$ Sliding takes place as $u(t)$ further reduces from $u^* - 2\phi$. We can use the above observation to identify those Jenkins elements that are sliding as the system reaches a value of $u(t)$. This causes us to further divide Eq. (39):

$$F(u(t)) = \int_0^{[u^*-u(t)]/2} \phi\ \rho(\phi)d\phi + \int_{[u^*-u(t)]/2}^{u^*} \left[u(t) - (u^* - \phi)\right]\rho(\phi)d\phi + K_{u^*}u(t). \tag{45}$$

With the above-presented definition of F^* (Eq. (43)), this can be written as

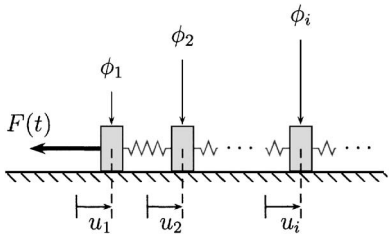

Fig. 4 Discrete model

$$F(u(t)) - F^* = -2\int_0^{[u^*-u(t)]/2} \phi\ \rho(\phi)d\phi + (u(t) - u^*)\left[K_{u^*} + \int_{[u^*-u(t)]/2}^{u^*} \rho(\phi)d\phi\right] \tag{46a}$$

$$= -2\int_0^{[u^*-u(t)]/2} \phi\ \rho(\phi)d\phi + (u(t) - u^*)\left[K_0 - \int_0^{[u^*-u(t)]/2} \rho(\phi)d\phi\right] \tag{46b}$$

Selecting $\rho(\phi) = (2+\chi)\phi^\chi$ for small values of ϕ, to provide power-law dissipation at low forces, Eq. (46*b*) becomes

$$F(u(t)) - F^* = \frac{2}{1+\chi}\left(\frac{u^* - u(t)}{2}\right)^{2+\chi} - K_0(u^* - u(t)) \tag{47}$$

Subtracting off the elastic term, this expression is similar to the force-displacement curve derived form the series-series continuum model, given in Eq. (36). In addition, the frictional dissipation per forcing cycle may be expressed as

$$D = \frac{4}{(1+\chi)(3+\chi)}(u^*)^{3+\chi} \tag{48}$$

As discussed in Segalman [11], in the micro-slip regime the gross displacement of the Iwan system is dominated by the elastic response, so that $u^* \sim F^*$. Therefore, comparing this equation for the parallel-series model with the equivalent expression for the continuum rod, given in Eq. (29), we find that the exponents of the distributions can be related as

$$\chi = \frac{1}{\beta} - 1, \quad \beta = \frac{1}{1+\chi}$$

Therefore, either the series-series or the parallel-series formulation may be used to generate power-law dissipation scalings arising from micro-slip. Segalman constructed a parallel-series Iwan model to have this power-law behavior at low and medium amplitude loads and other desirable properties at high loads [17].

3 Discrete Formulation

Although the above-described quasi-static continuum model can in principle be solved in closed form for arbitrary load histories, the requirement of keeping track of the slip reversal location can be cumbersome. This issue is obviated by considering the corresponding discrete series of Jenkins elements. The direct solution of the resulting nonlinear algebraic equations is notoriously awkward. We have chosen to regularize the problem by returning the intertial terms and solving a differential problem in time. Thus we are led to consider an n-degree-of-freedom discrete approximation to the continuum model given in Eq. (6) as shown in Fig. 4. The quasi-static result is recovered in the limit of forcing frequencies much less than one (the characteristic frequency of the system). This finite degree-of-freedom system corresponds to an

n-element series-series Iwan model. The discretization is obtained by a collocation method with quadratic comparison functions and in the following, the displacements are represented as

$$u_i(t) = u(x_i,t) \quad \text{with} \quad x_i = \frac{i}{n}\left(i - \frac{1}{2}\right), \quad i = 1,\ldots,n \tag{49}$$

With this, the discrete equations of motion become

$$\begin{aligned}
\frac{1}{n}\ddot{u}_1 + n(u_1 - u_2) &= \frac{G_1}{n} - F(t),\\
\frac{1}{n}\ddot{u}_2 + n(-u_1 + 2u_2 - u_3) &= \frac{G_2}{n},\\
&\vdots\\
\frac{1}{n}\ddot{u}_j + n(-u_{j-1} + 2u_j - u_{j+1}) &= \frac{G_j}{n},\\
&\vdots\\
\frac{1}{n}\ddot{u}_n + n\left(-\frac{4}{3}u_{n-1} + 4u_n\right) &= \frac{G_n}{n},
\end{aligned} \tag{50}$$

The description of the friction force G_i follows from the continuum model, i.e.,

$$G_i(t) = \begin{cases} -\phi_i \operatorname{sgn}(\dot{u}(t)), & \dot{u}_i(t) \neq 0,\\ -\min\left(|\mathcal{G}_i^{\text{eq}}(t)|, \phi_i\right)\operatorname{sgn}(\mathcal{G}_i^{\text{eq}}(t)), & \dot{u}_i(t) = 0, \end{cases} \tag{51}$$

where $\phi_i = \phi(x_i)$ and $\mathcal{G}_i^{\text{eq}}$ represents the force required to maintain static equilibrium on the i-th element. In particular, $\mathcal{G}_1^{\text{eq}}$ reduces to

$$\mathcal{G}_1^{\text{eq}} = n^2(u_1 - u_2) + nF(t), \tag{52}$$

so that in this discrete model, the boundary ($i=1$) element cannot support an equilibrium state if

$$\left|(u_1 - u_2) + \frac{F(t)}{n}\right| > \frac{\phi_1}{n^2}, \tag{53}$$

and in the undeformed configuration ($u_i=0$) the boundary element begins to slip if $F(t) \geqslant \phi_1/n$. As n increases, the minimum force necessary to induce initial slip decreases to zero. A similar model was considered in [18].

Our focus in this work is to characterize the effect of distributed friction, as represented by the number of discrete masses in the model, on the dynamic response of the interface as well as the energy dissipated by the frictional forces. To accomplish this, we investigate the response of the above-presented systems to external forces of the form:

$$F(t) = \alpha \sin(\tau), \quad \tau = \omega t + \tau(0) \tag{54}$$

and over one complete forcing cycle, τ varies over 2π regardless of the forcing frequency. The following numerical investigations are restricted to $0 < \omega \ll 1$ and $0 < \alpha \ll 1$, which correspond to physically common values of these nondimensional parameters. The results shown in the following are often represented as a function of τ rather than time. Finally, the instantaneous (nondimensional) power dissipated by the frictional forces can be expressed as

$$P_{\text{loss}}(t) = \frac{1}{n}\sum_{i=1}^{n} G_i(t)\dot{u}_i(t), \tag{55}$$

while the frictional work is calculated as the integral of this power over time.

The numerical results were obtained using a fourth-order Runge-Kutta method, with an integration step size of $\Delta t = 0.001/n$. Coulomb friction is incorporated through a regularized model proposed by Quinn [19]. To verify the accuracy of the results, the step size was reduced by a factor of 100 and the resulting simulated behavior showed no qualitative change (Fig. 4).

In Fig. 5(*a*) the dynamical behavior of the joint is shown for $\omega = 0.25$, $\alpha = 0.25$, and $n = 64$. In the figure the displacement of each element is traced versus τ, where the leftmost curve represents the terminal end of the chain (to which the forcing is applied). The asymptotic response is shown for one forcing cycle; the transient behavior (not shown) was removed by integrating over five forcing cycles before showing the results. Although this external load is one-quarter of that expected to initiate slip in the 1-dof model, a slip zone is seen at the end of the chain. However, only the 25 elements nearest the boundary of the rod experience slip—the majority of the joint remains stationary throughout the forcing cycle. In addition, the evolution of the slip interface is consistent with that predicted from the quasi-static continuum model described in the previous section.

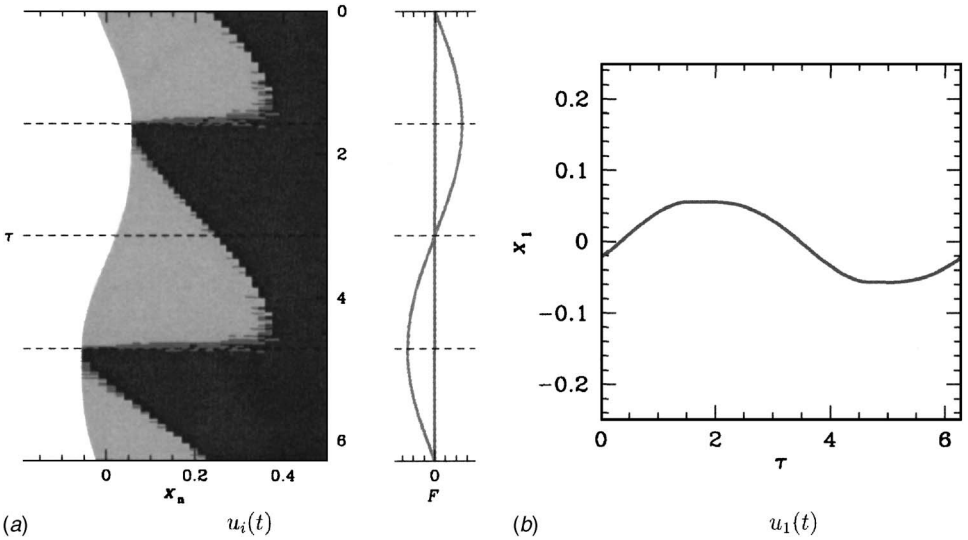

Fig. 5 Interfacial behavior with $n=64$ ($\omega=0.25$, $\alpha=0.25$). The displacements have been marked according to the slip velocity—for the lightest points $|\dot{u}_i| > v_0$ and for the darker points $v_0 > |\dot{u}_i| > v_0^2/n$. The velocity of the darkest points is $v_0^2/n > |\dot{u}_i|$, with $v_0 = 2\omega(\Delta t) = 7.8125 \times 10^{-6}$. The slip velocity is in the same direction as that of the end of the interface.

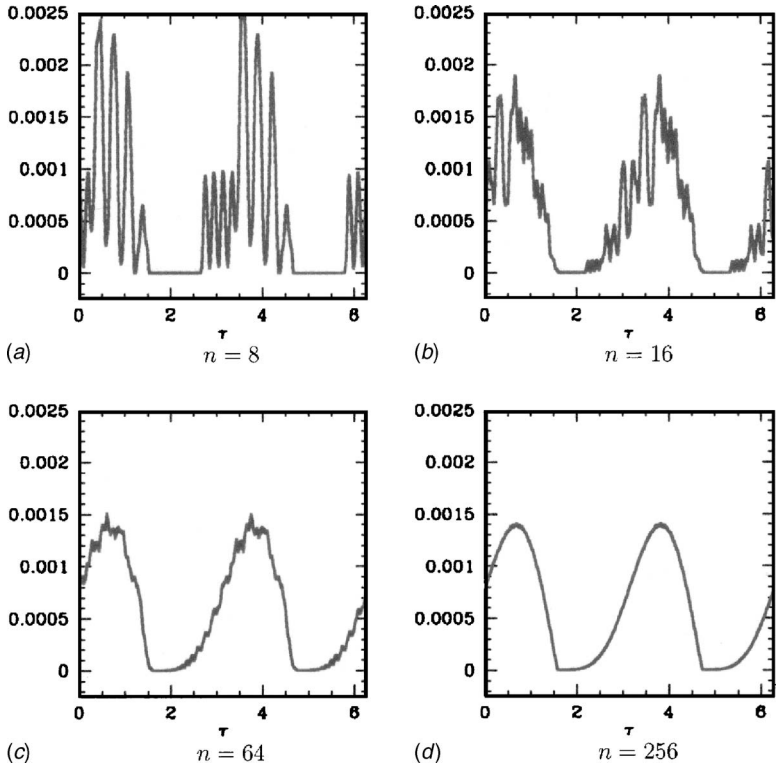

Fig. 6 Power dissipated over one steady-state cycle, $t=\omega\tau(\omega=0.25, \alpha=0.25)$

The power dissipated by the frictional forces is sensitive to the number of elements in the model. In Fig. 6 the power dissipated is shown over one cycle of motion for $n=8$, 16, 64, and 256. In the simulation the rod was initially at rest in an undeformed state, and then integrated for five cycles of the external forcing to remove the transient behavior before generating the observed figures. As the number of elements is decreased, the trace of the power dissipated becomes less smooth. For $n=256$ the trace of the instantaneous power dissipation is relatively smooth, while as the degree of freedom is decreased to $n=8$, power is dissipated in relatively short, large amplitude bursts, indicating significant stick-slip motions.

Surprisingly, the total work done per unit cycle is rather insensitive to the number of elements, provided a sufficient number are chosen to admit a time-dependent state, i.e., $n>1/\alpha$. In Fig. 7 the frictional work per unit cycle is shown as the number of elements varies from $n=2$ to $n=32$. As n increases beyond 32, the work remains fairly constant. For example, at $n=32$, the work is found to be $W=-0.015233$ while as n is increased to 256, the frictional work becomes $W=-0.015070$, which represents a 1.1% change for an eightfold increase in model size. Moreover, the dissipation predicted by the quasi-static continuum model is $W=-0.014882$ (see Eq. (29)).

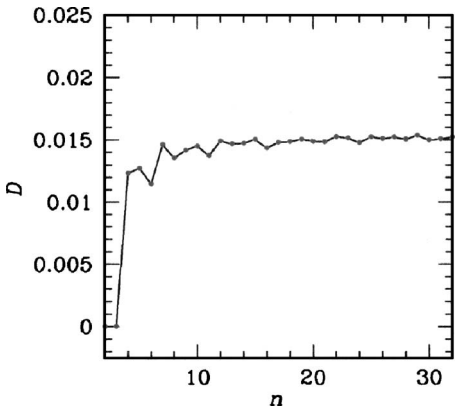

Fig. 7 Frictional dissipation per unit cycle as n varies ($\omega=0.25, \alpha=0.25$)

In contrast to variations in n, the work done by the frictional forces is strongly dependent on α. In Fig. 8(a), the frictional work is shown as α is varied, holding $\omega=0.25$ and $n=256$ fixed. As illustrated in the figure, the dissipation is well-represented by a power law and for this simulation the slope of this curve is approximately $m=2.672$. The numerical value closely approximates the predicted value of $m=8/3$ obtained from the quasi-static continuum model.

The work done by frictional forces can also be evaluated as the forcing frequency varies. In Fig. 8(b) both n and α are held fixed while $0.01<\omega<0.25$. Although some dependence on ω is seen ($m=0.002$), it is slight compared with the variation seen in W as α is varied. This implies that for forcing frequencies much less than the lowest characteristic frequency of the joint, the dissipation predicted by the quasi-static continuum model closely approximates the response predicted by the model with inertia. Moreover, the dissipation predicted by the discrete model rapidly approaches that of the quasi-static continuum model as the number of degrees-of-freedom (n) increases, provided that n is sufficient to resolve the slipping at the free end of the chain.

4 Discussion and Conclusions

We have considered an elastic rod sliding on a frictional surface subject to an external force across the structure. When the rod is assumed massless, the continuum partial differential equations can be solved exactly, based only on the amplitude of external force across the rod. This solution can then be used to predict the frictional dissipation and generate force-displacement curves for

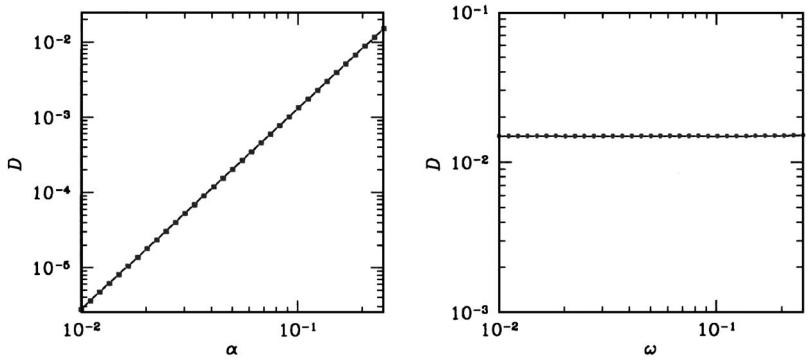

Fig. 8 Frictional work per unit cycle (n=256). The quantity m, represents the slope of this curve, as determined from linear regression

comparison with experimental data. When mass is included, the partial differential equations are discretized to develop a finite degree-of-freedom model.

The above-noted system is appropriate for the modeling of dissipation induced by mechanical joints, provided the forcing amplitude and frequency are limited. If the degrees-of-freedom of the discrete model is sufficiently large (roughly twice the value necessary to allow for micro-slip, c f., Eq. (53)), the predictions of the massless continuum model agree with those of the discrete formulation for the frictional dissipation per unit cycle. Moreover, in both formulations the dissipation per cycle is seen to depend sensitively on the distribution of the normal load over the rod, while for the parameter ranges applicable to joint dynamics it is insensitive to the frequency of the external loading.

Finally, this model yields power-law behavior in the dissipation per forcing cycle. Specifically, if the normal traction varies as x^{α} near the free edge of the rod, then the frictional dissipation per cycle scales with the forcing amplitude to a power of $(3+2\alpha)/(1+\alpha)$. As a special case, if the normal traction follows a Hertzian distribution, so that $\alpha=1/2$, the dissipation per cycle scales with the forcing amplitude to the 8/3 power which is similar to experimentally observed results [6,7]. These results indicate that the model under consideration is a reasonable first step toward the development of physically based reduced-order models for the incorporation of interfaced-induced dissipation in larger structural models.

References

[1] Mindlin, R. D., and Deresiewicz, H., 1953, "Elastic Spheres in Contact Under Varying Oblique Forces," ASME J. Appl. Mech., **20**, p. 327.

[2] Johnson, K. L., 1985, *Contact Mechanics*, Cambridge University Press, Cambridge.

[3] Dohner, J. L., 2001, "On the Development of Methodologies for Constructing Predictive Models of Structures with Joints and Interfaces," Tech. Rep. SAND2001-0003P, Sandia National Laboratories.

[4] Berger, E. J., Begley, M. R., and Mahajani, M., 2000, "Structural Dynamic Effects on Interface Response: Formulation and Simulation Under Partial Slipping Conditions," ASME J. Appl. Mech., **67**, pp. 785–792.

[5] Heinstein, M., and Segalman, D. J., 2001, "Bending Effects in the Energy Dissipation of Bolted Interfaces," presented at the 2001 ASME Design Engineering Technical Conferences, Pittsburgh, PA. September 9–12, DETC2001/VIB-21517.

[6] Gregory, D. L., Smallwood, D. O., Coleman, R. G., and Nusser, M. A., 1999, "Experimental Studies to Investigate Damping in Frictional Shear Joints," *Proceedings of the 70th Shock and Vibration Symposium.*

[7] Smallwood, D. O., Gregory, D. L., and Coleman, R. G., 2000, "Damping Investigations of a Simplified Frictional Shear Joint," Tech. Rep. SAND2000-1929C, Sandia National Laboratories.

[8] Goodman, L. E., and Brown, C. B., 1962, "Energy Dissipation in Contact Friction: Constant Normal and Cyclic Tangential Loading," ASME J. Appl. Mech., **29**, p. 17.

[9] Iwan, W. D., 1966, "A Distributed-element Model for Hysteresis and Its Steady-state Dynamic Response," ASME J. Appl. Mech., **33**, pp. 893–900.

[10] Iwan, W. D., 1967, "On a Class of Models for the Yielding Behavior of Continuous and Composite Systems," ASME J. Appl. Mech., **89**, pp. 612–617.

[11] Segalman, D. J., 2001, "An Initial Overview of Iwan Modeling for Mechanical Joints," Tech. Rep. SAND2001-0811, Sandia National Laboratories.

[12] Tworzydlo, W. W., Cecot, W., Oden, J. T., and Yew, C. H., 1998, "Computational Micro- and Macroscopic Models of Contact and Friction: Formulation, Approach and Applications," Wear, **220**, pp. 113–140.

[13] Dankowicz, H., 1999, "On the Modeling of Dynamic Friction Phenomena," Z. Angew. Math. Mech., **79** (6), pp. 399–409.

[14] Ruina, A. L., 1983, "Slip Instability and State Variable Friction Laws," J. Geophys. Res., **88** (B12), pp. 10359–10370.

[15] Menq, C.-H., Bielak, J., and Griffin, J. H., 1986, "The Influence of Microslip on Vibratory Response, Part I: A New Microslip Model," J. Sound Vib., **107**, pp. 279–293.

[16] Menq, C.-H., Griffin, J. H., and Bielak, J., 1986, "The Influence of Microslip on Vibratory Response, Part II: A Comparison with Experimental Results," Sound Vib., **107**, pp. 295–307.

[17] Segalman, D. J., 2002, "A Four-parameter Iwan Model for Lap-type Joints," Tech. Rep. SAND2002-3828, Sandia National Laboratories.

[18] Quinn, D. D., 2001, "Distributed Friction and Microslip in Mechanical Joints with Varying Degrees-of-freedom," presented at the 2001 ASME Design Engineering Technical Conferences, Pittsburgh, PA. September 9-12, DETC2001/VIB-21514.

[19] Quinn, D. D., 2004, "A New Regularization of Coulomb Friction," ASME J. Vibr. Acoust., **126**, pp. 391–397.